

Calibration-based abundances in the interstellar gas of galaxies from slit and IFU spectra

L. S. Pilyugin^{1,2}, M. A. Lara-López^{3,4}, J. M. Vílchez⁵, S. Duarte Puentes^{6,5}, I. A. Zinchenko^{7,2}, and O. L. Dors Jr.⁸

¹ Institute of Theoretical Physics and Astronomy, Vilnius University, Sauletekio av. 3, 10257, Vilnius, Lithuania

² Main Astronomical Observatory, National Academy of Sciences of Ukraine, 27 Akademika Zabolotnoho St, 03680, Kiev, Ukraine

³ Departamento de Física de la Tierra y Astrofísica, Universidad Complutense de Madrid, E-28040 Madrid, Spain

⁴ Instituto de Física de Partículas y del Cosmos IPARCOS, Fac. de Ciencias Físicas, Univ. Complutense de Madrid, E-28040, Madrid, Spain

⁵ Instituto de Astrofísica de Andalucía, CSIC, Apdo 3004, 18080 Granada, Spain

⁶ Département de Physique, de Génie Physique et d'Optique, Université Laval, and Centre de Recherche en Astrophysique du Québec (CRAQ), Québec, QC, G1V 0A6, Canada

⁷ Faculty of Physics, Ludwig-Maximilians-Universität, Scheinerstr. 1, 81679 Munich, Germany

⁸ Universidade do Vale do Paraíba, Av. Shishima Hifumi, 2911, Cep 12244-000, São José dos Campos, SP, Brazil

September 29, 2022

ABSTRACT

In this work we make use of available Integral Field Unit (IFU) spectroscopy and slit spectra of several nearby galaxies. The pre-existing empirical R and S calibrations for abundance determinations are constructed using a sample of H II regions with high quality slit spectra. In this paper, we test the applicability of those calibrations to the IFU spectra. We estimate the calibration-based abundances obtained using both the IFU and the slit spectroscopy for eight nearby galaxies. The median values of the slit and IFU spectra-based abundances in bins of 0.1 in fractional radius R_g (normalized to the optical radius R_{25}) of a galaxy are determined and compared. We find that the IFU and the slit spectra-based abundances obtained through the R calibration are close to each other, the mean value of the differences of abundances is 0.005 dex and the scatter in the differences is 0.037 dex for 38 datapoints. The S calibration can produce systematically underestimated values of the IFU spectra-based abundances at high metallicities ($12 + \log(\text{O}/\text{H}) \gtrsim 8.55$), the mean value of the differences is -0.059 dex for 21 datapoints, while at lower metallicities the mean value of the differences is -0.018 dex and the scatter is 0.045 dex for 36 data points. This evidences that the R calibration produces more consistent abundance estimations between the slit and the IFU spectra than the S calibration. We find that the same calibration can produce close estimations of the abundances using IFU spectra obtained with different spatial resolution and different spatial samplings. This is in line with the recent finding that the contribution of the diffuse ionized gas to the large aperture spectra of H II regions has a secondary effect.

Key words. galaxies: abundances – ISM: abundances – H II regions, galaxies

1. Introduction

The investigation of the relations between gas-phase abundance and other characteristics of galaxies is very important in understanding the (chemical) evolution of galaxies. In addition to the obtained relations being affected by the absolute abundance values (i.e. metallicity scale), which depends on the adopted method for the abundance determinations, a mandatory condition in constructing such relations is for the abundances of all the galaxies to be on a unique metallicity scale. This implies that the abundances should be determined through a single method or through methods producing abundances on the same metallicity scale. If abundances obtained through a given method depend on the way of the spectral measurements (e.g. on a part of the H II region measured) then the emission line spectra of H II regions in galaxies should be measured in similar way.

The emission line spectra of H II regions in galaxies available at the present day are measured in different ways. The long slit spectra of H II regions in many galaxies were obtained in numerous investigations (e.g. see compilations in Pilyugin et al. 2004, 2014; Zurita et al. 2021). Strictly speaking, the slit spectra are not uniform in the sense that the physical fraction of H II region within the slit can significantly vary for different reasons: *i*)

because of variations on the slit widths in different works, *ii*) because of variation in angular sizes of the H II regions (due to the variation on the physical sizes of H II regions and/or distances to galaxies), *iii*) because the slit can cross different parts (centre or periphery) of H II regions. One can adopt (at least, as the first order approximation) that the variations in different parts of H II regions measured in the slit spectroscopy are random.

The Integral Field Unit (IFU) spectroscopy measurements of the galaxy NGC 628 were carried out within the PPAK Integral Field Spectroscopy Nearby Galaxies Survey, PINGS, (Sánchez et al. 2011; Rosales-Ortega et al. 2011). The 382 fibre bundle has a field of view (FoV) of a hexagonal shape of $74 \text{ arcsec} \times 64 \text{ arcsec}$. Each fibre projects to $2''.7$ in diameter on the sky, and the fibre-to-fibre distance is $3''.2$, which yields a total filling factor of 0.6. A dithering scheme with three pointings has been used to cover the complete FoV of the bundle. The spatial resolution of full width at half maximum (FWHM) is $\sim 2.5 \text{ arcsec}$. The catalog of H II regions in NGC 628 is generated, and the spectra of detected H II regions are extracted (Rosales-Ortega et al. 2011). The angular size of a nearby galaxy usually exceeds the diameter of the field of view of the spectrograph. Therefore a

number of pointings are observed to form a mosaic, for instance, Sánchez et al. (2011) obtained 34 pointings for the NGC 628.

The IFU spectroscopy measurements of a sample of galaxies on the nearby Universe are carried out in the same way (and using the same instrument as in PINGS) within the Calar Alto Legacy Integral Field Area (CALIFA) survey (Sánchez et al. 2012, 2016; García-Benito et al. 2015). Those observations are used to construct a grid of spectra with a spatial sampling of $1''$ and/or to detect H II regions and extract their spectra. The recent version of the catalogue of H II regions involves 924 galaxies¹ (Espinosa-Ponce et al. 2020).

The fibre spectra were measured in many galaxies within the Sloan Digital Sky Survey (SDSS, York et al. (2000)). The SDSS spectra are obtained through a 3-arcsec diameter fibres. In the framework of the SDSS IV programme, the IFU spectroscopy for 10000 galaxies are carried out within the Mapping Nearby Galaxies at Apache Point Observatory (MaNGA) survey (Bundy et al. 2015). The diameters of the fields of view vary from $12''$ (19 fibres) to $32''$ (127 fibres). A final spatial sampling is $0''.5/\text{pixel}$, the point spread function (PSF) of the MaNGA measurements is estimated to have a full width at half maximum of 2.5 arcsec or 5 pixel (Bundy et al. 2015; Belfiore et al. 2017). The wavelength interval covers from 3600 to 10300 Å with the spectral resolution $R \sim 2000$.

A sample of nearby spiral galaxies (within ~ 20 Mpc) are measured within the PHANGS (Physics at High Angular Resolution in Nearby Galaxies) programme, using the Very Large Telescope/Multi Unit Spectroscopic Explorer (VLT/MUSE) to mosaic the central disk of galaxies with optical IFU observations within a $1'0 \times 1'0$ field of view with $0''.2$ pixels and a typical spectral resolution of $\sim 2.5\text{Å}$ over the wavelength range covering 4800–9300 Å (Kreckel et al. 2019). The angular resolution between galaxies varies from $0''.5$ to $1'0$.

An integral field spectroscopic survey of a sample of 30 nearby spiral galaxies with the Mitchell Spectrograph (formerly called VIRUS-P) IFU on the 2.7 metre telescope at McDonald Observatory, was carried out within the framework of the VIRUS-P Exploration of Nearby Galaxies (VENGA) survey (Blanc et al. 2013; Kaplan et al. 2016). The Mitchell Spectrograph has large field of view ($1'7 \times 1'7$). Each fibre is $4''.2$ in diameter, the spatial resolution is 5.6 arcsec (full width half-maximum, FWHM). Each galaxy was observed with both a blue (3600–5800 Å) and red (4600–6800 Å) setup to obtain a wide wavelength coverage. The spectral resolution is $R \sim 1000$ at 5000 Å, which corresponds to ~ 120 km/s. Using the same instrument, the IFU spectroscopy of THINGS galaxies (Walter et al. 2008) is under observational campaigns as part of the Metal-THINGS survey (Lara-López et al. 2021, 2022). Some galaxies are observed with both a blue and red setups, however the red spectra is observed for all galaxies.

It is widely accepted that the direct T_e method produces reliable estimations of the abundances in H II region. The auroral lines necessary for the application of the direct T_e method for the abundance determinations are measured in the long slit spectra of H II regions. The amount of spectra of H II regions with detected auroral lines is steadily growing. Nevertheless the use of the different variants of the strong line method (calibrations) is the dominant way for the estimations of the abundances in the interstellar gas in galaxies. The H II regions with abundances determined through the direct method and the strong emission line fluxes measured in their spectra are used

as the calibrating data points in the construction of the empirical calibrations (e.g. Pilyugin 2000, 2001b; Pettini & Pagel 2004; Pilyugin & Thuan 2005; Pilyugin & Mattsson 2011; Marino et al. 2013; Pilyugin & Grebel 2016; Curti et al. 2017). Since those empirical calibrations are based on the slit spectra then the applicability of that calibrations for the abundance determinations using the IFU spectra can be questioned.

Indeed, a spatial resolution and an angular size of the native spatial sample (fibre or spaxel) can significantly exceed the angular size of H II regions. If this is the case then the diffuse ionized gas (DIG) outside H II regions can make a contribution to the fibre (spaxel) spectrum as well to the extracted spectrum of the H II region. However, Mannucci et al. (2021) found that the difference between the spectra local H II regions and more distant galaxies is not due to contamination from the DIG, but by the smaller angular size of the slit with respect to the projected size of the H II regions, and hence the DIG has a secondary effect. Indeed, H II regions are stratified in the sense that higher ionization species dominate the inner regions of nebulae while lower ionization species are more abundant in the outer parts (see Figure 1 in Mannucci et al. (2021) or Figure 3 in Pérez-Montero et al. (2014)). Therefore, the spectra from small apertures show differences from the spectra when larger apertures are used, even if still inside the H II regions.

The goal of the current work is to examine the compatibility or disagreement between the calibration-based abundances obtained using the slit spectra of H II regions and the IFU spectra of spatial samplings (fibres) or extracted IFU spectra of H II regions. The three-dimensional R calibration $(O/H)_R = f(R_2, N_2, R_3/R_2)$ and S calibration $(O/H)_S = f(N_2, S_2, R_3/S_2)$ from Pilyugin & Grebel (2016) are considered. There is no one-to-one correspondence between positions and apertures of the slit and IFU sampling. We determine the median value for abundances in bins of 0.1 in R/R_{25} and the scatter of each bin for both the slit and the IFU spectra-based abundances. The use of median value in bins (the abundances at a given galactocentric distances) provides a possibility to compare the slit and IFU spectra-based abundances.

Throughout the paper, we will use the following standard notations for the line intensities:

$$R_2 = I_{[O\ II]\lambda 3727 + \lambda 3729} / I_{H\beta},$$

$$N_2 = I_{[N\ II]\lambda 6548 + \lambda 6584} / I_{H\beta},$$

$$S_2 = I_{[S\ II]\lambda 6717 + \lambda 6731} / I_{H\beta},$$

$$R_3 = I_{[O\ III]\lambda 4959 + \lambda 5007} / I_{H\beta}.$$

We also use the standard notation for electron temperature $t_e = 10^{-4}T_e$. The galactocentric distance of H II region or spatial sampling is given as a fractional radius R_g normalized to the optical radius R_{25} of a galaxy, $R_g = R/R_{25}$.

2. Oxygen abundances in galaxies based on spectral measurements of different types

2.1. NGC 5457: comparison between $(O/H)_{T_e}$, $(O/H)_R$, and $(O/H)_S$ abundances based on the slit spectra

The giant nearby galaxy NGC 5457 (M 101, the Pinwheel) is a prototype of the Sc spiral galaxies (morphological type code T = 5.9 ± 0.3). NGC 5457 is a face-on galaxy, its inclination angle is $i = 18^\circ$ and the position angle of the major axis PA = 37° (Kamphuis 1993). The optical radius of NGC 5457 is $R_{25} = 14.42$ arcmin or 865.2 arcsec (de Vaucouleurs et al. 1991).

There are 79 independent distance measurements for NGC 5457 after the year 2000 including those using Cepheids and tip of the red giant branch (TRGB) (Lomeli-Núñez et al.

¹ http://ifs.astroscu.unam.mx/CALIFA/HII_regions/new_catalogs/

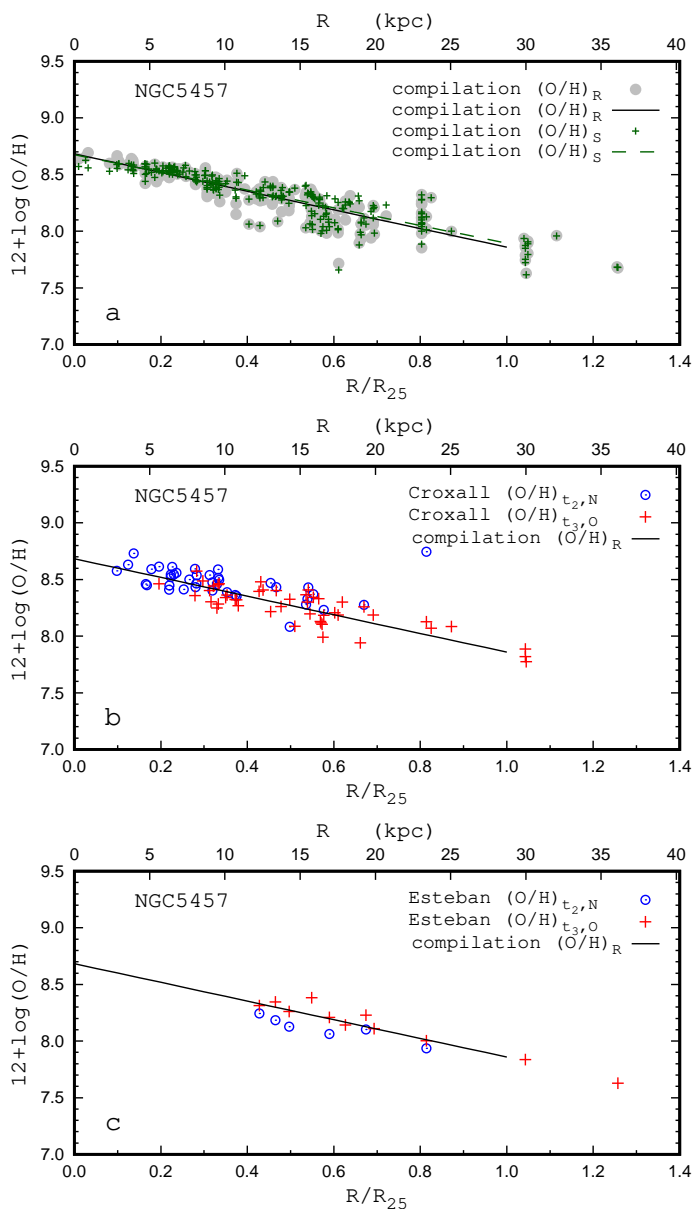


Fig. 1. Radial oxygen abundance distribution in NGC 5457. *Panel a:* calibration-based oxygen abundances for the compilation of the slit spectra of H II regions. The grey circles denote the $(O/H)_R$ abundances for individual measurements, the black solid line is the best linear fit to those data. The green plus signs are the $(O/H)_S$ abundances for individual measurements, the dashed line is the best linear fit to those data. *Panel b:* T_e -based oxygen abundances with measured electron temperatures $t_{2,N}$ (circles) and $t_{3,O}$ (plus signs) in H II regions from Croxall et al. (2016). The solid line is the $(O/H)_R - R$ relation from panel a. *Panel c:* the same as panel b but for the sample of H II regions from Esteban et al. (2020).

2022). The obtained distances are within the range ~ 6 to ~ 9 Mpc. We adopt here the distance to NGC 5457 $d = 6.85$. Each characteristic of NGC 5457 is rescaled if necessary to the distance adopted here. The optical radius of NGC 5457 is $R_{25} = 28.73$ kpc with the adopted distance.

The oxygen abundance distribution across the disk of NGC 5457 is considered in a number of investigations (Kennicutt & Garnett 1996; Kennicutt et al. 2003; Pilyugin 2001a; Croxall et al. 2016; Esteban et al. 2020, and references therein). Since the auroral lines were measured in the spectra of a number of its H II regions and, consequently, the abundances

in those H II regions can be derived through the direct T_e method, then NGC 5457 has been used to test the validity of the calibrations, i.e., in some sense NGC 5457 can be considered as a “Rosetta stone” (Pilyugin & Grebel 2016). Recent measurements of H II regions spectra (including the auroral lines) in NGC 5457 are published by Croxall et al. (2016) and Esteban et al. (2020). This provides an additional possibility to compare the abundances produced by the empirical calibrations with the direct abundances. It should be noted that the measurements from Croxall et al. (2016) and Esteban et al. (2020) were not used in constructing of the R and S calibrations, however, the spectra of H II regions of NGC 5457 with detectable auroral lines from other publications were used.

The upper panel of Fig. 1 shows the oxygen abundances estimated through the R and S calibration from Pilyugin & Grebel (2016) as a function of radius for the compilation of the slit spectra of H II regions in NGC 5457 (measurements from Croxall et al. (2016) and Esteban et al. (2020) are added to the compilation in Pilyugin & Grebel (2016)). The grey points denote the $(O/H)_R$ abundances of individual H II regions, the black solid line is the best linear fit to those data. The green plus signs are the $(O/H)_S$ abundances of individual H II regions, the dashed line is the best fit to those data.

It is believed that the T_e method, based on the measurements of temperature-sensitive line ratios, should give accurate oxygen abundances. In practice, however, T_e -based oxygen abundances in the same H II region derived in different works can differ because of two reasons. First, there may be errors in the line intensity measurements. Second, the T_e -based oxygen abundances depend on the realization of the T_e method, i.e. the derived abundances depend on the relations used to convert the values of the line fluxes to the electron temperatures and to the ion abundances. The determined abundances depend also on the adopted relationship between electron temperature in low-ionization zones and electron temperatures in high-ionization parts of nebula. The differences between the oxygen abundances at a given H II region produced by different realizations of the T_e method can be appreciable (Yates et al. 2020; Cameron et al. 2021). For example, Esteban et al. (2017) found an oxygen abundance of $12 + \log(O/H)_{T_e} = 8.14 \pm 0.05$ in the Galactic H II region Sh 2-83, while Arellano-Córdova et al. (2020) found $12 + \log(O/H)_{T_e} = 8.28 \pm 0.08$ in the same H II region using the same spectroscopic measurements. Berg et al. (2015) detected the auroral lines in 45 H II regions in the nearby galaxy NGC 628. They determine the T_e -based abundances in those H II regions and estimate the radial abundance gradient. They found the central (intersect) oxygen abundance $12 + \log(O/H)_0 = 8.83 \pm 0.07$ in the NGC 628. However, in their recent paper, Berg et al. (2020) recalculate ionic and total T_e -based abundances in those H II regions and determine the central (intersect) oxygen abundance $12 + \log(O/H)_0 = 8.71 \pm 0.06$ for the same galaxy.

The calibration-based abundances in H II regions of NGC 5457 are determined above through the R and S calibrations from Pilyugin & Grebel (2016). The T_e -based oxygen abundances in H II regions used as the calibrating data points in the construction of those calibrations are derived using the T_e -method equations reported in Pilyugin et al. (2012). In order for the calibration-based and the T_e -based abundances correspond to a unique abundance scale, the T_e -based oxygen abundances for the H II regions in NGC 5457 are determined here using the T_e -method equations from Pilyugin et al. (2012). It should be emphasized that we do not pretend that the T_e -based abundances in NGC 5457 recomputed here are more accurate than the original abundances in the cited papers. We only take care that

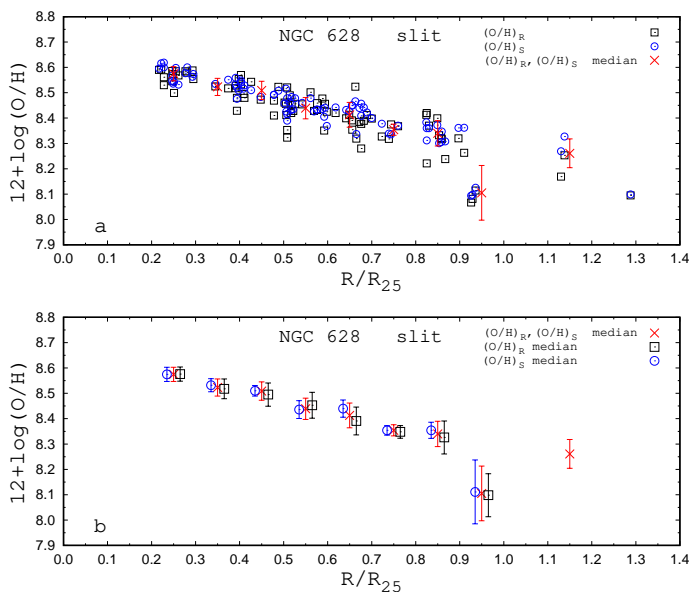


Fig. 2. Radial distribution of the slit spectra-based oxygen abundances in NGC 628. *Panel a*: squares denote the abundances estimated through the R calibration for individual measurements, circles are the S calibration-based abundances. The crosses mark the median value for $(O/H)_R$ and $(O/H)_S$ together in bins of 0.1 in R/R_{25} and the scatter of each bin. *Panel b*: the median value for the $(O/H)_S$ (circles), for the $(O/H)_R$ (squares), and for the $(O/H)_R$ and the $(O/H)_S$ together (crosses). The median values for different abundances are obtained for the same bin, but the positions of symbols (circles and squares) are slightly shifted along the X axis for clarity.

all the abundances used here correspond to the same metallicity scale. If the measurements of two auroral lines ($[O\ III]\lambda 4363$ and $[N\ II]\lambda 5755$) are available for the H II region then two values of the electron temperature ($t_{3,O}$ and $t_{2,N}$) can be derived and, consequently, two independent values of the oxygen abundance ($(O/H)_{t_{3,O}}$ and $(O/H)_{t_{2,N}}$) can be estimated. If the electron temperature in the low-ionized part of the nebula $t_2 = t_{2,N}$ is measured then the electron temperature in the high-ionization part of the nebula $t_3 = t_{3,O}$ is obtained using the relationships between electron temperatures in the nebula, and conversely.

Panel b of Fig. 1 shows the T_e -based oxygen abundances of NGC 5457 H II regions from Croxall et al. (2016). The oxygen abundances obtained using the measured electron temperatures $t_{2,N}$ are shown by circles and those for the measured electron temperatures $t_{3,O}$ by plus signs. The $(O/H)_R - R_g$ relation from panel a of Fig. 1 is shown by the solid line. Panel c of Fig. 1 shows the oxygen abundances of NGC 5457 H II regions from Esteban et al. (2020).

Inspection of the Fig. 1 suggests that the radial abundance gradients traced by the T_e -based, R and S calibration-based abundances determined from the slit spectra are in a satisfactory agreement to each other. Therefore the slit spectra-based abundances determined through the R and S calibrations can be used as the reference abundances.

2.2. NGC 628: comparison between abundances based on slit and IFU spectra

2.2.1. Slit spectra-based abundances in NGC 628

The nearby galaxy NGC 628 (M 74, the Phantom Galaxy) is an isolated Sc spiral galaxy (morphological type code T = 5.2 ± 0.5). NGC 628 is a face-on galaxy, its inclination angle

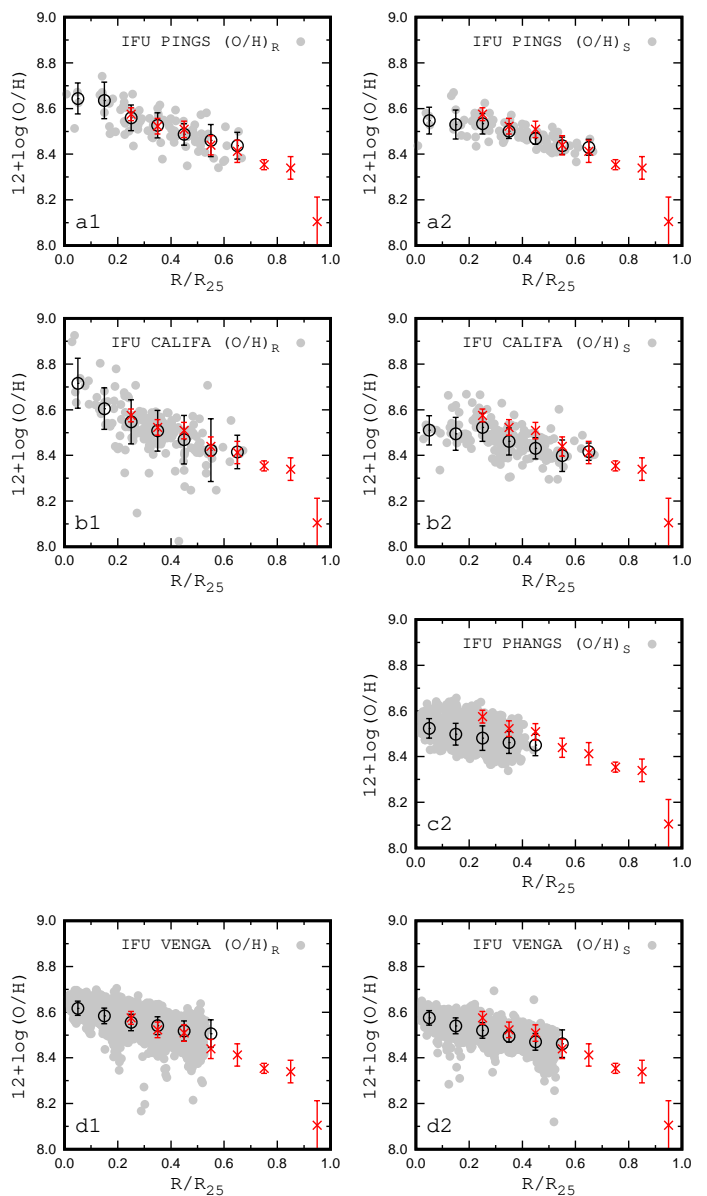


Fig. 3. Radial distributions of the oxygen abundances in NGC 628. *Panels of columns 1-2*: radial distributions of abundances estimated through the R calibration (column 1) and S calibration (column 2). *Panels of rows a-d*: abundances based on the IFU measurements from PINGS (row a), from CALIFA survey (row b), from PHANGS survey (row c), and from VENGA survey (row d). The grey points denote the abundances for the individual H II regions (panels of rows a, b, c) or individual spatial samplings (panels of row d), the dark circles mark the median value in bins of 0.1 in R/R_{25} and the scatter of each bin. The red crosses in each panel designate the median values for the slit spectra-based abundances ($(O/H)_R$ and $(O/H)_S$ together) and comes from Fig. 2.

is $i = 6^\circ$ and the position angle of the major axis $PA = 25^\circ$ (Kamphuis & Briggs 1992). The optical radius of this galaxy is $R_{25} = 5.24$ arcmin or 314.1 arcsec (de Vaucouleurs et al. 1991). The H I disk extends out to more than three times the optical radius (Kamphuis & Briggs 1992). There are recent distance estimations for NGC 628 through the tip of the red giant branch (TRGB) method based on the Hubble Space Telescope measurements. Jang & Lee (2014) find the distance to NGC 628 to be 10.19 ± 0.14 (random) ± 0.56 (systematic) Mpc. McQuinn et al (2017) measure the distance to M74 to be 9.77 ± 0.17 (statistical uncertainty) ± 0.32 (systematic uncertainty) Mpc. Sabbi et al.

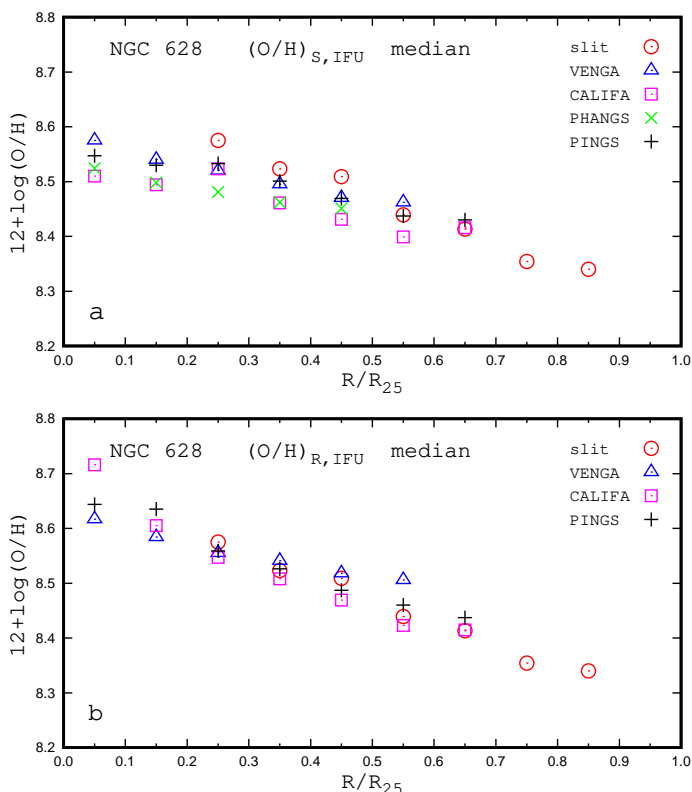


Fig. 4. The median values of oxygen abundances in bins of NGC 628. *Panel a:* median values of $(O/H)_S$ abundances based on the IFU measurements from PINGS (plus signs), from CALIFA survey (squares), from PHANGS survey (crosses), and from VENGA survey (triangles). The median values of the abundances based on the slit measurements (circles) are obtained for the $(O/H)_S$ and $(O/H)_R$ abundances together. *Panel b:* the same as panel a but for the $(O/H)_R$ abundances.

(2018) determine the distances for the central pointing ($d = 8.6 \pm 0.9$ Mpc) and for the outer field ($d = 8.8 \pm 0.7$ Mpc). We adopt here the distance to the NGC 628 used in our previous paper ($d = 9.91$ Mpc (Pilyugin et al. 2014)) which is close to the values obtained by Jang & Lee (2014) and McQuinn et al (2017). The optical radius of NGC 628 is $R_{25} = 15.09$ kpc with adopted distance.

The slit spectra of the H II regions in the NGC 628 were measured in a number of early works (McCall et al. 1985; Ferguson et al. 1998; van Zee et al. 1998; Bresolin et al. 1999), and the slit spectroscopy of H II regions in NGC 628 were carried out within the framework of the CHEMICAL Abundances Of Spirals (CHAOS) project (Berg et al. 2015).

Squares in panel a of Fig. 2 show the oxygen abundances estimated through the R calibration in individual H II regions and circles are the S calibration-based abundances. The median values of the $(O/H)_R$ and the $(O/H)_S$ together in bins of 0.1 in R/R_{25} are denoted by crosses, the bar marks the scatter in each bin. Panel b of Fig. 2 show the comparison between median values for the $(O/H)_S$ (circles), for the $(O/H)_R$ (squares), and for the $(O/H)_R$ and the $(O/H)_S$ together (crosses). The median values for different abundances are obtained for the same bin, but the positions of symbols (circles and squares) are slightly shifted along the X axis for clarity. Inspection of panel b of Fig. 2 shows that the differences between median value for $(O/H)_S$ (or $(O/H)_R$) abundances and the median value for the $(O/H)_S$ and the $(O/H)_R$ abundances together is less than the uncertainties of median values. This justifies the use of the median value for

the $(O/H)_S$ and the $(O/H)_R$ abundances together instead of the median values for the $(O/H)_S$ or the $(O/H)_R$ abundances separately to specify the abundance in bin in the case of the slit spectra-based abundances. The advantages of such approach are the following. First. In this case, the IFU spectra-based $(O/H)_S$ and $(O/H)_R$ abundances are compared with the same reference (slit spectra-based) abundances. Second. The slit spectra measurements for a galaxy are usually a few in number (see below). Therefore, the use of $(O/H)_S$ and $(O/H)_R$ abundances together provides a possibility to estimate the median values in larger number of bins than for the $(O/H)_S$ or the $(O/H)_R$ abundances only.

Thus, in the case of the slit spectra-based abundances, we will estimate and use the median value in the bin for the $(O/H)_S$ and the $(O/H)_R$ abundances together and will notate those median values as $(O/H)_{SLIT}$.

2.2.2. IFU spectra-based abundances in NGC 628

Rosales-Ortega et al. (2011) identify H II regions and extract their spectra from the IFU measurements. They generate the H II regions catalog for NGC 628 (PINGS catalog). The oxygen abundances in the H II regions catalog from Rosales-Ortega et al. (2011) are obtained via the R calibration are denoted by grey circles in panel a1 of Fig. 3. The dark circles mark the median value in bins of 0.1 in R/R_{25} and the scatter of each bin. The red crosses designate the median values in bins for the slit spectra-based abundances ($(O/H)_R$ and $(O/H)_S$ together) and comes from Fig. 2. Panel a2 of Fig. 3 shows the oxygen abundances in the H II regions from Rosales-Ortega et al. (2011) estimated through the S calibration (grey points), and the dark circles mark the median value in bins and the scatter of each bin.

Espinosa-Ponce et al. (2020) have also constructed a catalog of H II regions in the NGC 628 using IFU observations (CALIFA catalog). The oxygen abundance in H II regions of the CALIFA catalog obtained through the R calibration are denoted by grey circles in panel b1 of Fig. 3, The dark circles are the median values in bins, and the bar shows the scatter of each bin. The grey circles in panel b2 of Fig. 3 are the oxygen abundances in those H II regions estimated through the S calibration and the dark circles are the median values in bins.

The IFU spectroscopy of the central part of NGC 628 were carried out within the framework of the PHANGS programme using the Very Large Telescope (Kreckel et al. 2019). The catalog of the H II regions in NGC 628 was created on the base of those measurements. Unfortunately only the red spectra over the wavelength range covering 4800-9300Å were obtained. Since the line $[O II]\lambda\lambda 3727,3729$ is not measured then the R calibration cannot be applied to those H II regions. The grey points in panel c2 of Fig. 3 denote the oxygen abundances in individual H II regions estimated through the S calibration, and the dark circles are the median values in bins.

The IFU (fibre) spectroscopy of NGC 628 was performed within the framework of the VENGA survey (Blanc et al. 2013; Kaplan et al. 2016). The oxygen abundance in the individual fibres obtained through the R calibration are denoted by grey circles in panel d1 of Fig. 3. The grey circles in panel d2 of Fig. 3 are the oxygen abundances in the fibres estimated through the S calibration. The dark circles in both panels mark the median value in bins and the scatter of each bin.

We compare the abundances in NGC 628 obtained from IFU spectra from different surveys to each other and to the slit spectra-based abundances in Fig. 4. Panel a shows the median

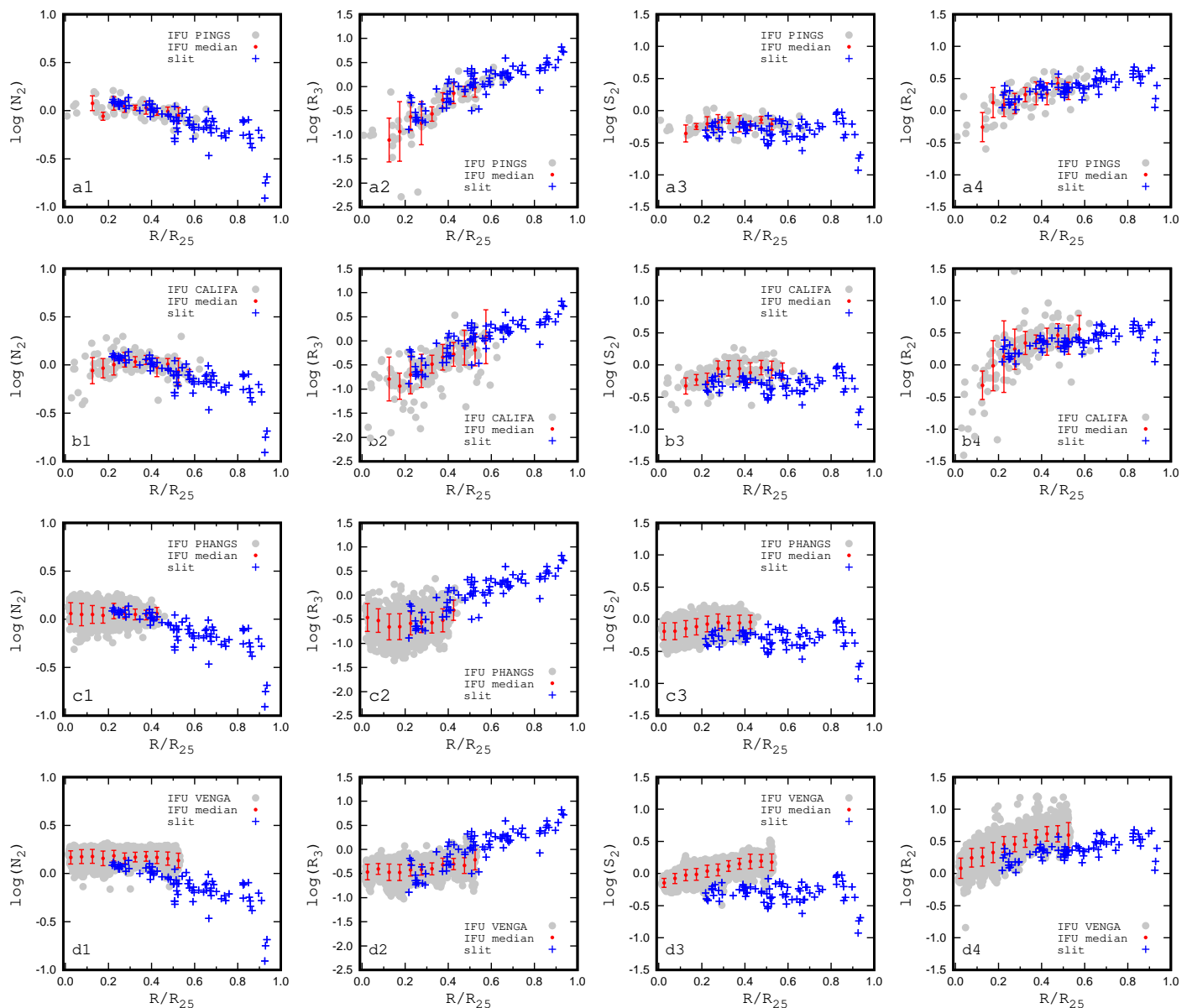


Fig. 5. Radial distributions of the emission line fluxes in NGC 628. *Panels of columns 1-4:* radial distributions of intensities of N_2 line (column 1), R_3 line (column 2), S_2 line (column 3), and R_2 line (column 4). *Panels of rows a-d:* IFU measurements from the surveys PINGS (row a), CALIFA (row b), PHANGS (row c), and VENGA (row d). The grey points denote the individual H II regions (panels of rows a, b, c) or individual spatial samplings (panels of row d), the red points with bars mark the median value in bins of 0.05 in R/R_{25} and the scatter of each bin. The blue plus signs are individual slit measurements. Since only the red spectra were measured within the PHANGS programme then the R_2 line measurements are not available.

values of $(O/H)_S$ abundances based on the IFU measurements from PINGS (plus signs), from CALIFA survey (squares), from PHANGS survey (crosses), and from VENGA survey (triangles). The median values of the abundances based on the slit measurements (circles) are obtained for the $(O/H)_S$ and $(O/H)_R$ abundances together. Panel b shows a similar comparison for the $(O/H)_R$ abundances.

Easeman et al. (2022) find that central dips in the metallicity profiles within galaxies can be observed using spatially resolved IFU data. It is not clear whether the dips are real or they are an artefact introduced by the strong line diagnostics used to determine the metallicity. The radial changes of the $(O/H)_S$ abundances based on the PINGS and the CALIFA IFUs measurements are not perfectly monotonic, panels a2 and b2 in Fig. 3. However, it is not clear whether the deviation from the

monotonoc trend is caused by the decrease in the central metallicity (at $R/R_{25} \lesssim 0.2$) or by the enhancement of the metallicity in the only bin, at $R/R_{25} = 0.2$ to 0.3 . If this bin is ignored then the metallicity profile becomes monotonic. Moreover the radial changes of the $(O/H)_S$ abundances based on the PHANGS and the VENGA IFUs measurements are monotonic, panels c2 and d2 in Fig. 3. Thus, the central dip in the metallicity profile within the NGC 628 is unlikely.

Inspection of the panels of columns 1 and 2 in Fig. 3 and Fig. 4 shows the following.

- The $(O/H)_R$ abundances based on the IFU spectra of H II regions from PINGS and CALIFA and spectra of fibres from VENGA are in agreement to each other and to the slit spectra-based abundances.
- The $(O/H)_S$ abundances based on the IFU spectra of H II re-

gions from PINGS, CALIFA, and PHANGS and on the IFU spectra of fibres from VENGA are more or less similar. The IFU spectra-based $(O/H)_S$ abundances are close to the slit spectra-based abundances at large galactocentric distances but there is difference at smaller galactocentric distances (at high metallicities) in the sense that the IFU spectra-based $(O/H)_S$ abundances are lower than the slit spectra-based abundances. As a result, the radial abundance gradient traced by the $(O/H)_S$ abundances based on the IFU spectra is flatter than that for abundances based on the slit spectra. Belfiore et al. (2017) find that the galaxy inclination generates a flattening on the radial abundance gradient, since flux from different galactocentric radii is summed up when the galaxy is projected in the plane of the sky. The metallicity depletion at the galaxy centre depends on the PSF and galaxy inclination and can be as large as ~ 0.02 dex. Since NGC 628 is a face-on galaxy (with inclination $i = 6^\circ$) then this effect should be minor.

Unfortunately, the slit spectra measurements are not available at the central region ($R/R_{25} \lesssim 0.2$) of NGC 628 while the IFU spectra are not available at larger radii ($R/R_{25} \gtrsim 0.65$). Therefore, the comparison is possible within the restricted interval of galactocentric distances only.

Comparison between the emission line fluxes in the slit and IFU spectra in NGC 628 can clarify the origin of the difference in abundances. Fig. 5 shows the radial distributions of the emission line fluxes in the slit and the IFU spectra in NGC 628. The grey points denote the individual IFU spectra of H II regions (panels of rows a, b, and c) or individual fibres (panels of row d), the red points with bars mark the median value in the bins of 0.05 in R/R_{25} and the scatter of each bin. The blue plus signs are individual slit spectra. The differences between the emission line fluxes in the slit and IFU spectra result in the differences between the slit spectra-based and the IFU spectra-based abundances.

The difference in S_2 (and other lines) between different IFU measurements cannot be attributed to the difference in the spatial resolution only. If this would be the case then one could expect that the S_2 for a given galaxy (e.g. NGC 628) should be similar in the CALIFA and PINGS IFUs since the spatial and spectral resolutions are the same. But there is an appreciable difference between S_2 from those surveys (compare panels a3 and b3 in Fig. 5). Then one can assume that the reduction of the observations (e.g. extraction of H II region spectra) and flux calibration, can contribute to the uncertainty in the IFU spectra and, as consequence, can produce some differences in the S_2 measurements between different IFUs. However, the general behaviour of the IFU spectra-based abundances are more or less similar for different IFUs.

It may appear that $(O/H)_{S,IFU} - (O/H)_{SLIT}$ is larger than $(O/H)_{R,IFU} - (O/H)_{SLIT}$ (Fig. 3 and Fig. 4) because of the larger differences in the S_2 flux measured between the IFU and the slit spectra. However, close examination of the available data reveals that differences in other lines fluxes must also play a significant role. For example, we find that the differences in the S_2 flux between PINGS and VENGA are larger than between PINGS and CALIFA (Fig. 5), but the differences in $(O/H)_S$ between PINGS and VENGA are smaller than that between PINGS and CALIFA (Fig. 3 and Fig. 4). Moreover, at $R/R_{25} = 0.45$ to 0.50, the median values of the R_2 and S_2 fluxes in CALIFA and PINGS agree within $\sim 10\%$ and $\sim 25\%$, respectively, and the difference between the median values of $(O/H)_R$ and $(O/H)_S$ are ~ 0.01 dex and ~ 0.05 dex, respectively. Whereas, at $R/R_{25} = 0.15$ to 0.20, the median values of the R_2 and S_2 fluxes in CALIFA and PINGS agree within $\sim 25\%$ and $\sim 10\%$, respectively, but the difference between the median values of $(O/H)_R$ and $(O/H)_S$

are ~ 0.02 dex and ~ 0.03 dex, respectively. This suggests that the abundances obtained through the S calibration are affected by variations in the line fluxes more strongly than abundances obtained through the R calibration.

From one side, since the spatial resolutions (and sizes of the native spatial samplings) of PHANGS, CALIFA, PINGS, and VENGA observations are appreciable different then one can expect that the spectra of the extracted H II regions in PHANGS should be less contaminated by the DIG than the spectra of the extracted H II regions in PINGS and CALIFA and than the spectra of spatial samplings in VENGA. From other side, the shifts of the $(O/H)_S$ abundances based on the IFU spectra of PHANGS, CALIFA, PINGS, and VENGA in comparison to the slit spectra-based abundances are rather close to each other. Those two facts taken together are in line with the conclusion of Mannucci et al. (2021) that the DIG has a secondary effect.

Thus, the investigation of the galaxy NGC 628 can be summarized as following. *i*) the oxygen abundance estimated from the IFU spectra of the extracted H II regions, or from the IFU spectra of fibres, depends weakly on the spatial resolution (and size of the native spatial samplings) of the IFU measurements. *ii*) the R calibration applied to the IFU spectra produce more consistent abundance estimations between slit and IFU spectra than the S calibration, the $(O/H)_{S,IFU}$ abundances are systematically underestimated in comparison with the slit spectra-based abundances at high metallicities. *iii*) the satisfactory agreement between abundances estimated from the IFU spectra obtained with different spatial resolutions (and different sizes of the native spatial samplings) confirm the recent finding of Mannucci et al. (2021) that the DIG has a secondary effect. To confirm or reject those conclusions, seven other nearby galaxies with available slit and IFU spectroscopy are examined (see Appendix A).

3. Discussion

Here we compare and discuss the abundances based on the slit spectra and the abundances determined from the IFU spectra using the R and the S calibrations. There are 38 bins of 0.1 in R/R_{25} in eight galaxies considered where the median values of both $(O/H)_{R,IFU}$ and $(O/H)_{SLIT}$ abundances are determined and 57 bins where the median values of both $(O/H)_{S,IFU}$ and $(O/H)_{SLIT}$ abundances are determined (Fig. 3, Fig. A.1 – Fig. A.7).

In panel a1 of Fig. 6 we plot the abundance determined from the IFU spectra through the S calibration in individual bins as a function of the abundance obtained from the slit spectra for all eight galaxies, and in panel b1 of Fig. 6 we plot the $(O/H)_{R,IFU}$ abundance against the $(O/H)_{SLIT}$ abundances. The grey points in panel a2 of Fig. 6 are the abundances in individual bins (the same data as in panel a1) and the dark circles mark the mean value in bins of 0.05 in $\log(O/H)_{SLIT}$ for those data points. Panel b2 of Fig. 6 shows the diagram similar to that in panel a2 but for the $(O/H)_{R,IFU}$ abundances.

Fig. 7 shows the normalized histograms of the differences between oxygen abundances $(O/H)_{R,IFU} - (O/H)_{SLIT}$ for 38 data points (solid line) and between $(O/H)_{S,IFU} - (O/H)_{SLIT}$ for 57 data points (dashed line). The step in the histograms is 0.02 dex.

Inspection of panel a1 of Fig. 6 and Fig. 7 shows that the differences between $(O/H)_{SLIT}$ and $(O/H)_{S,IFU}$ abundances are usually less than around 0.1 dex, the mean value of the scatter in abundance differences $(O/H)_{S,IFU} - (O/H)_{SLIT}$ is 0.052 dex for the 57 data points. However, the differences are not perfectly random, the maximum of the distribution is appreciable

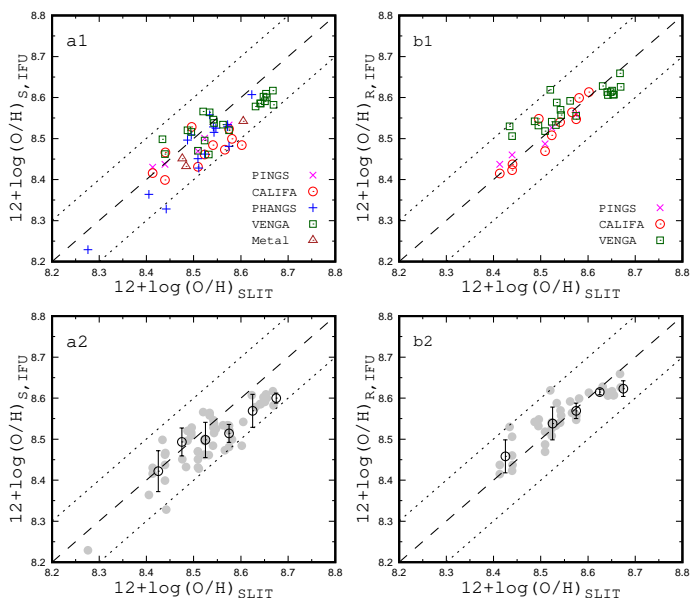


Fig. 6. Comparison between the abundances based on the slit spectra of H II regions, and the abundances estimated from the IFU spectra of H II regions (or spatial samplings, fibres) using the R and the S calibrations. *Panel a1*: IFU spectra-based oxygen abundances (median values in bins) obtained through the S calibration vs. oxygen abundances estimated from the slit spectra for our sample of galaxies. Each point shows the median value in bin of 0.1 in R/R_{25} in galaxy (Fig. 3, Fig. A.1 – Fig. A.7). The abundances based on the IFU spectra from different surveys are shown by different symbols. The solid line indicates the one-to-one relation; while the dashed lines show the ± 0.1 dex deviation. *Panel b1*: the same as panel a1 but for the IFU spectra-based abundances estimated through the R calibration. *Panel a2*: grey points are data from panel a1, the dark circles mark the mean value in bins of 0.05 in $\log(O/H)$ for those data points. *Panel b2*: the same as panel a2 but for the IFU spectra-based abundances estimated through the R calibration.

shifted from zero, Fig. 7. Examination of panels a1 and a2 of Fig. 6 shows that the $(O/H)_{S,IFU}$ abundances are systematically lower than the $(O/H)_{SLIT}$ abundances at high metallicities ($12 + \log(O/H) \gtrsim 8.55$), the mean shift of the $(O/H)_{S,IFU}$ abundances relative to the $(O/H)_{SLIT}$ abundances is -0.059 dex for 21 data points, that is the shift of $(O/H)_{S,IFU}$ abundances relative to the $(O/H)_{SLIT}$ abundances at high metallicities exceeds the mean value of the scatter in the abundance differences.

Inspection of panel b1 of Fig. 6 and Fig. 7 shows that the differences between $(O/H)_{SLIT}$ and $(O/H)_{R,IFU}$ abundances are also within 0.1 dex, the mean value of the scatter in abundance differences $(O/H)_{R,IFU} - (O/H)_{SLIT}$ is 0.037 dex for the 38 data points. One can observe that the correlation between $(O/H)_{R,IFU}$ and $(O/H)_{SLIT}$ abundances is more tight than the correlation between $(O/H)_{S,IFU}$ and $(O/H)_{SLIT}$ abundances. The maximum of the abundance differences distribution is close to zero, Fig. 7. Nevertheless, close examination of panels b1 and b2 of Fig. 6 shows that some correlation between the abundance difference $(O/H)_{R,IFU} - (O/H)_{SLIT}$ and metallicity can exist. However, the mean shift of the $(O/H)_{R,IFU}$ abundances relative to the $(O/H)_{SLIT}$ abundances exceeds the scatter in abundance differences for one metallicity interval ($12 + \log(O/H)$ from 8.65 to 8.70) only. Therefore it is not clear whether this weak correlation is meaningful.

Inspection of panel a1 of Fig. 6 shows that there is an agreement between the $(O/H)_{S,IFU}$ estimated from the IFU measurements obtained with different spatial resolutions, and panel b1 shows such agreement for the $(O/H)_{R,IFU}$ abundances. This

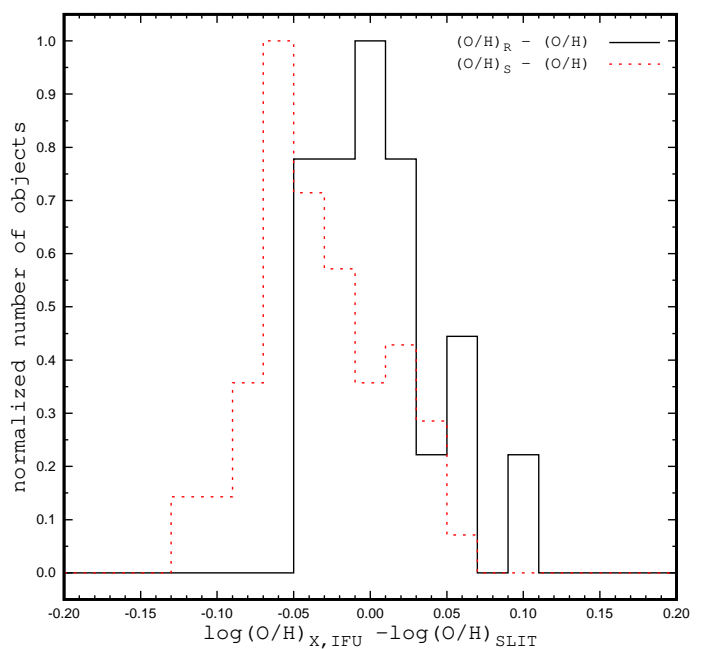


Fig. 7. The normalized histograms of the differences between oxygen abundances $(O/H)_{R,IFU} - (O/H)_{SLIT}$ (solid line) and $(O/H)_{S,IFU} - (O/H)_{SLIT}$ (dashed line).

suggests that the IFU spectra-based abundances depend weakly (if any) on the spatial resolution of the IFU measurements. Indeed, there is an agreement between the $(O/H)_{S,IFU}$ abundances estimated in NGC 4254 from the VENGA measurements (panel b in Fig. A.5) and from the PHANGS measurements (panel d in Fig. A.5) although the spatial resolution of the VENGA measurements is significantly lower than that of the PHANGS measurements. Moreover, the agreement between $(O/H)_{S,IFU}$ abundances estimated in NGC 628 from the PINGS and the VENGA measurements obtained with different spatial resolutions is better than the agreement between $(O/H)_{S,IFU}$ abundances estimated from the PINGS and the CALIFA measurements obtained with the same spatial resolution, Fig. 4.

Thus, the analysis of a sample of nearby galaxies confirms the conclusions reached above when considering the galaxy NGC 628. It should be emphasized that the abundances analysed here are distributed over the limited interval of metallicity, from $12 + \log(O/H) \sim 8.4$ to ~ 8.7 only (with one exception). In order to strengthen (or reject) our conclusions and derive the relationships between the IFU and slit spectra-based abundances, one needs the abundances distributed over the larger diapason of metallicity.

4. Conclusions

The calibration-based abundances are considered in eight nearby galaxies where both, the slit spectra of H II regions and the spectra of H II regions extracted from the IFU measurements (PINGS, CALIFA, and PHANGS surveys) or the IFU spectra of spatial samplings (VENGA and Metal-THINGS surveys) are available. The pre-existing empirical R and S calibrations for abundance determinations are constructed using a sample of H II regions with high quality slit spectra (Pilyugin & Grebel 2016). In this study, we test the applicability of those calibrations to the IFU spectra. We estimate the R and S calibration-based abundances using both the IFU and the slit spectroscopy for eight nearby galaxies. The median values of the IFU spectra-based

abundances $(O/H)_{R,IFU}$ and $(O/H)_{S,IFU}$ in bins of 0.1 in fractional radius R_g (normalized to the optical radius R_{25}) of a galaxy are determined and compared to the median values of the slit spectra-based abundances $(O/H)_{SLIT}$ determined using both the $(O/H)_R$ and $(O/H)_S$ abundances together.

We find that the differences between $(O/H)_{SLIT}$ and $(O/H)_{S,IFU}$ abundances are usually less than around 0.1 dex, the mean value of the scatter in abundance differences $(O/H)_{S,IFU} - (O/H)_{SLIT}$ is 0.052 dex for the 57 data points. However, the $(O/H)_{S,IFU}$ abundances are systematically lower than the $(O/H)_{SLIT}$ abundances at high metallicities ($12 + \log(O/H) \gtrsim 8.55$), the mean shift of the $(O/H)_{S,IFU}$ abundances relative to the $(O/H)_{SLIT}$ abundances is around -0.06 dex for 21 data points. The difference between the intensities of each line (used in the abundance determinations) in the slit and the IFU spectra contributes to the difference between the abundances based on the slit and the IFU spectra. Our data indicates that the abundances estimated through the S calibration are more sensitive to the variations in the line fluxes than the abundances obtained using the R calibration.

The correlation between $(O/H)_{R,IFU}$ and $(O/H)_{SLIT}$ abundances is more tight than the correlation between $(O/H)_{S,IFU}$ and $(O/H)_{SLIT}$ abundances, the mean value of the scatter in abundance differences $(O/H)_{R,IFU} - (O/H)_{SLIT}$ is 0.037 dex for the 38 data points. There is hint that the weak correlation between the abundance difference $(O/H)_{R,IFU} - (O/H)_{SLIT}$ and metallicity can exist. However, the mean shift of the $(O/H)_{R,IFU}$ abundances relative $(O/H)_{SLIT}$ abundances is less than the scatter in abundance differences for any (except one) metallicity interval of 0.05 dex. Therefore it is not clear whether this weak correlation is meaningful.

We find that the same calibration can produce a close estimations of the abundances using the IFU spectra (of extracted H II regions or spatial samplings) from the IFU measurements carried out with different spatial resolution and different native spatial samplings. This is in line with the finding in Mannucci et al. (2021) that the contribution of the diffuse ionized gas to the large aperture spectra of H II regions has a secondary effect.

Acknowledgements

We are grateful to the referee for his/her constructive comments. We thank the VENGA collaboration for providing access to the data.

L.S.P acknowledges support from the Research Council of Lithuania (LMTLT) (grant no. P-LU-PAR-22-7).

MALL acknowledges support from the Spanish grant PID2021-123417OB-I00. SDP is grateful to the Fonds de Recherche du Québec - Nature et Technologies. JVM and SDP acknowledge financial support from the Spanish Ministerio de Economía y Competitividad under grants AYA2016-79724-C4-4-P and PID2019-107408GB-C44, from Junta de Andalucía Excellence Project P18-FR-2664, and also acknowledge support from the State Agency for Research of the Spanish MCIU through the ‘Center of Excellence Severo Ochoa’ award for the Instituto de Astrofísica de Andalucía (SEV-2017-0709).

This study makes use of the results based on the Calar Alto Legacy Integral Field Area (CALIFA) survey (<http://califa.caha.es/>).

References

Anand G.S., Lee J.C., Van Dyk S.D., et al., 2021, MNRAS, 501, 3621

- Arellano-Córdova K.Z., Esteban C., García-Rojas J., Méndez-Delgado J.E., 2020, MNRAS, 496, 1051
- Belfiore F., Maiolino R., Tremonti C., et al., 2017, MNRAS, 469, 151
- Berg D.A., Skillman E.D., Croxall K.V., Pogge R.W., Moustakas J., Johnson-Groh M., 2015, ApJ, 806, 16
- Berg D.A., Pogge R.W., Skillman E.D., Croxall K.V., Moustakas J., Rogers N.S.J., Sun J., 2020, ApJ, 893, 96
- Blanc G.A., Schrubba A., Evans N.J., et al., 2013, ApJ, 764, 117
- Bresolin F., Kennicutt R.C., Garnett, D.R., 1999, ApJ, 510, 104
- Bresolin F., Garnett, D.R., Kennicutt R.C., 2004, ApJ, 615, 228
- Bresolin F., Schaerer D., González Delgado R.M., Stasińska G., 2005, A&A, 441, 981
- Bresolin F., 2019, MNRAS, 488, 3826
- Bundy K., Bershady M.A., Law D.R., et al., 2015, ApJ, 798, 7
- Cameron A.J., Yuan T., Trenti M., Nicholls D.C., Kewley L.J., 2021, MNRAS, 501, 3695
- Colombo D., Meidt S.E., Schinnerer E., et al., 2014, ApJ, 784, 4
- Croxall K.V., Pogge R.W., Berg D.A., Skillman E.D., Moustakas J., 2015, ApJ, 808, 42
- Croxall K.V., Pogge R.W., Berg D.A., Skillman E.D., Moustakas J., 2016, ApJ, 830, 4
- Curti M., Cresci G., Mannucci F., Marconi A., Maiolino R., Esposito S., 2017, MNRAS, 465, 1384
- Davis B.L., Berrier J.C., Johns L., et al., 2014, ApJ, 789, 124
- de Blok W.J.G., Walter F., Brinks E., Trachternach C., Oh S.-H., Kennicutt R.C., 2008, AJ, 136, 2648
- de Vaucouleurs G., de Vaucouleurs A., Corvin H.G., Buta R.J., Paturel J., Fouque P. 1991, Third Reference Catalog of bright Galaxies, New York: Springer Verlag (RC3)
- Díaz Á., Terlevich E., Vilchez J.M., Pagel B.E.J., Edmunds M., 1991, MNRAS, 253, 245
- Díaz Á., Terlevich E., Castellanos M., Hägele G., 2007, MNRAS, 382, 251
- Drozdzovsky I.O., Karachentsev I.D., 2000, A&AS, 142, 425
- Easeman B., Schady P., Wuyts S., Yates R.M., 2022, MNRAS, 511, 371
- Espinosa-Ponce C., Sánchez S.F., Morisset C., Barrera-Ballesteros J.K., Galbany L., García-Benito R., Lacerda E.A.D., Mast D., 2020, MNRAS, 494, 1622
- Esteban C., Fang X., García-Rojas J., Toribio San Cipriano, 2017, MNRAS, 471, 987
- Esteban C., Bresolin F., García-Rojas, Toribio San Cipriano, 2020, MNRAS, 491, 2137
- Ferguson A.M.N., Gallagher J.S., Wyse R. F. G. 1998, AJ, 116, 673
- García-Benito R., Díaz Á., Hägele G.F., et al., 2010, MNRAS, 408, 2234
- García-Benito R., Zibetti S., Sánchez S.F., et al., 2015, A&A, 576, A135
- García-Gómez C., Barberà C., Athanassoula E., Bosma A., Whyte L., 2004, A&A, 421, 595
- Garnett D., Kennicutt R.C., Bresolin F., 2004, ApJ, 607, L21
- Henry R.B.C., Pagel B.E.J., Chincarini G.L., 1994, MNRAS, 266, 421
- Jang I.S., Lee M.G., 2014, ApJ, 792, 52
- Jarrett T.H., Cluver M.E., Brown M.J.I., Dale D.A., Tsai C.W., Masci F., 2019, ApJS, 245, 25
- Kamphuis J.J., 1993, PhD Thesis, Univ. Groningen
- Kamphuis J., Briggs F., 1992, A&A, 253, 335
- Kaplan K.F., Jogee S., Kewley L., et al., 2016, MNRAS, 462, 1642
- Kennicutt R.C., Garnett D.R., 1996, ApJ, 456, 504
- Kennicutt R.C., Bresolin F., Garnett D.R., 2003, ApJ, 591, 801
- Kreckel K., Ho I.-T., Blanc G.A., et al., 2019, ApJ, 887, 80
- Lang P., Meidt S., Rosolowsky E., et al., 2020, ApJ, 897, 122
- Lara-López M., Zinchenko I., Pilyugin L., et al., 2021, ApJ, 906, 42
- Lara-López M., et al., 2022, submitted to A&A
- Leroy A.K., Walter F., Brinks E., Bigiel F., de Blok W.J.G., Madore B., Thornley M.D., 2008, AJ, 136, 2782
- Leroy A.K., Sandstrom K., Lang D., et al., 2019, ApJS, 244, 24
- Leroy A.K., Schinnerer E., Hughes A., et al., 2021, ApJS, 257, 43
- Lomelí-Núñez L., Mayya Y.D., Rodríguez-Merino L.H., Ovando P.A., Rosa-González D., 2022, MNRAS, 509, 180
- Mannucci F., Belfiore F., Curti M., Cresci G., Maiolino R., Marasco A., Marconi A., Mingozzi M., Tozzi G., Amiri A., 2021, MNRAS, 508, 1582
- Marino R.A., Rosales-Ortega F.F., Sánchez S.F., et al., 2013, A&A, 559, A114
- McCall M.L., Rybski P.M., Shields G.A., 1985, ApJS, 57, 1
- McQuinn K.B.W., Skillman E.D., Dolphin A.E., Berg D., Kennicutt R., 2017, AJ, 154, 51
- Pérez-Montero E., Monreal-Ibero A., Relaño M., Vilchez J.M., Kehrig C., Morisset C., 2014, A&A, 566, A12
- Pettini M., Pagel B.E.J., 2004, MNRAS, 348, L59
- Pilyugin L.S., 2000, A&A, 362, 325
- Pilyugin L.S., 2001a, A&A, 373, 56
- Pilyugin L.S., 2001b, A&A, 369, 594
- Pilyugin L.S., Vilchez J.M., Contini T., 2004, A&A, 425, 849
- Pilyugin L.S., Thuan T.X., 2005, ApJ, 631, 231
- Pilyugin L.S., Mattsson L., 2011, MNRAS, 412, 1145

- Pilyugin L.S., Grebel E.K., Mattsson L., 2012, MNRAS, 424, 2316
Pilyugin L.S., Grebel E.K., Kniazev A.Y., 2014, AJ, 147, 131
Pilyugin L.S., Grebel E.K., 2016, MNRAS, 457, 3678
Rosales-Ortega F.F., Díaz A.I., Kennicutt R.C., Sánchez S.F., 2011, MNRAS, 415, 2439
Rots A.H., Bosma A., van der Hulst J.M., Athanassoula E., Crane P.C., 1990, AJ, 100, 387
Ryder S.D., 1995, ApJ, 444, 610
Sabbi E., Calzetti D., Ubeda L., et al., 2018, ApJS, 235, 23
Sánchez S.F., Rosales-Ortega F.F., Kennicutt R.C., Johnson B.D., Diaz A.I., Pasquali A., Hao C.N., 2011, MNRAS, 410, 313
Sánchez S.F., Kennicutt R.C., Gil de Paz A., et al., 2012, A&A, 538, A8
Sánchez S.F., García-Benito R., Zibetti S., et al., 2016, A&A, 594, A36
Schmidt B.P., Kirshner R.P., Eastman R.G., Phillips M.M., Suntzeff N.B., Hamuy M., Maza J., Aviles R., 1994, ApJ, 432, 42
Shields G.A., Skillman E.D., Kennicutt R.C., 1991, ApJ, 371, 825
Storchi-Bergmann T., Wilson A.S., Baldwin J.A., 1996, ApJ, 460, 252
Tamburro D., Rix H.-W., Walter F., Brinks E., de Blok W.J.G., Kennicutt R.C., Mac Low M.-M., 2008, AJ, 136, 2872
van den Bosch R.C.E., 2016, ApJ, 831, 134
van Zee L., Salzer J.J., Haynes M.P., O'Donoghue A.A., Balonek T.J., 1998, AJ, 116, 2805
Walter F., Brinks E., de Blok W.J.G., Bigiel F., Kennicutt R.C., Thornley M.D., Leroy A., 2008, AJ, 136, 2563
Yates R.M., Schady P., Chen T.-W., Schweyer T., Wiseman P., 2020, A&A, 634, A107
York D.G., Adelman J., Anderson J.E., et al., 2000, AJ, 120, 1579
Zurita A., Florido E., Bresolin F., Pérez-Montero E., Pérez I., 2021, MNRAS, 500, 2359

Appendix A: Abundances based on slit and IFU spectra in nearby galaxies

Here we estimate the oxygen abundances based on the slit and the IFU spectra in seven nearby galaxies with available slit and IFU spectroscopy. The $(O/H)_{R,IFU}$ and/or $(O/H)_{S,IFU}$ abundances for individual IFU spectra as well as the median abundances in bins of 0.1 in fractional radius R/R_{25} are determined. The median values of the slit spectra-based abundances $(O/H)_{SLIT}$ are determined using both the $(O/H)_R$ and the $(O/H)_S$ abundances for individual H II regions together. The median value is determined if the number of points in the bin is larger than 3. The abundances in each galaxy are shown below, Fig. A.1 – Fig. A.7. The data for that sample of galaxies (together with the data for NGC 628) are presented in Fig. 6 and Fig. 7 and are used in discussion.

Appendix A.1: NGC 1058

NGC 1058 is a Sc galaxy (morphological type code $T = 5.1 \pm 0.9$). The inclination angle of NGC 1058 is $i = 15^\circ$, the position angle of the major axis $PA = 145^\circ$ (García-Gómez et al 2004). The optical radius is 1.51 arcmin, or 90.6 arcsec (de Vaucouleurs et al. 1991). At the distance of $d = 10.6$ Mpc (Schmidt et al. 1994), the physical optical radius is $R_{25} = 4.66$ kpc. The stellar mass (rescaled to the adopted distance) is $M_\star = 2.51 \times 10^9 M_\odot$ (Leroy et al. 2019).

The slit spectra of H II regions in NGC 1058 were measured by Ferguson et al. (1998) and Bresolin (2019). The squares in panel a of Fig. A.1 show the oxygen abundances estimated through the R calibration in those H II regions. The circles in panel a of Fig. A.1 are the oxygen abundances in those H II regions estimated through the S calibration. The median values in bins of 0.1 in fractional radius R/R_{25} determined using both the $(O/H)_R$ and the $(O/H)_S$ abundances for individual H II regions together are denoted by crosses. The bar shows the scatter in each bin.

The IFU spectroscopy of NGC 1058 is carried out within the CALIFA survey. The grey points in panel b of Fig. A.1 show the IFU spectra-based $(O/H)_S$ abundances of H II regions as a function of radius in NGC 1058. The line flux measurements in the spectra of H II regions are taken from the catalog of H II regions (cited above). The median values in bins of 0.1 in fractional radius R/R_{25} are denoted by dark circles. The bar shows the scatter in each bin. Panel c of Fig. A.1 shows the same as panel b but for $(O/H)_{R22}$ abundances.

Appendix A.2: NGC 1672

NGC 1672 is a Sb galaxy (morphological type code $T = 3.3 \pm 0.6$). The inclination angle of NGC 1672 is $i = 43^\circ$, and the position angle of the major axis $PA = 134^\circ$ (Lang et al. 2020). The optical radius is 3.30 arcmin or 198.2 arcsec (de Vaucouleurs et al. 1991). At the distance of $d = 19.40$ Mpc (Anand et al. 2021), the physical optical radius is $R_{25} = 18.64$ kpc. The stellar mass is $M_\star = 5.37 \times 10^{10} M_\odot$ (Leroy et al. 2021). NGC 1672 hosts a central black hole of mass $\log M_{BH} = 7.08 \pm 0.90$ in solar mass (Davis et al. 2014).

The slit spectra of H II regions in NGC 1672 were measured by Storchi-Bergmann et al. (1996). The estimated $(O/H)_R$ and $(O/H)_S$ abundances in individual H II HII regions are shown in panel a of Fig. A.2 by squares and circles, respectively. The crosses are the median values in bins for those data. The IFU spectroscopy of NGC 1672 were carried out within the frame-

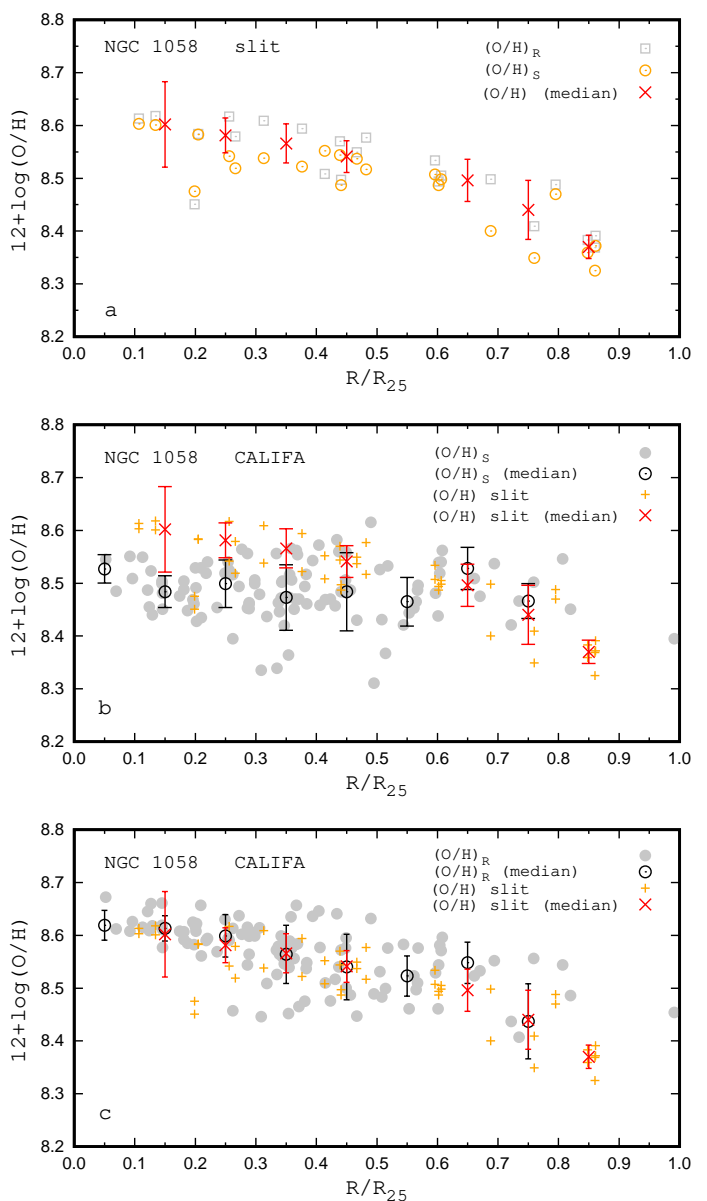


Fig. A.1. Radial oxygen abundance distribution in NGC 1058. *Panel a:* oxygen abundances based on the slit spectra of H II regions. The squares denote the abundances estimated through the R calibration for individual measurements, the circles designate the $(O/H)_S$ abundances. The crosses mark the median values of the slit spectra-based abundances in bins of 0.1 in the fractional radius determined using both the $(O/H)_R$ and the $(O/H)_S$ abundances for individual H II regions together. The bar shows the scatter in each bin. *Panel b:* grey points denote the $(O/H)_{S,IFU}$ abundances based on the extracted IFU (CALIFA) spectra of individual H II regions. The dark circles mark the median values in bins, and bar shows the scatter in each bin. The crosses mark the median values of the slit spectra-based abundances and come from panel a. *Panel c:* the same as panel a but for the $(O/H)_{R,IFU}$ abundances.

work of the PHANGS programme (Kreckel et al. 2019). The catalog of the H II regions in NGC 1672 was created on the base of those measurements. Unfortunately only the red spectra over the wavelength range covering 4800-9300Å were obtained. Since the line $[O II]\lambda\lambda 3727, 3729$ is not measured then the R calibration cannot be applied to those H II regions. The grey circles in panel b of Fig. A.2 denote the oxygen abundances in individ-

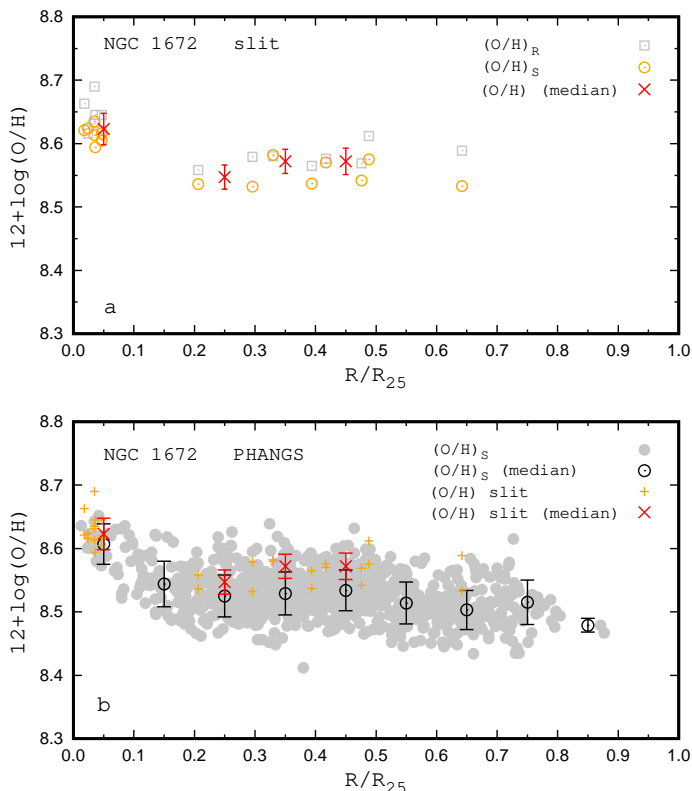


Fig. A.2. Radial oxygen abundance distribution in NGC 1672. *Panel a*: oxygen abundances based on the slit spectra of H II regions. *Panel b*: oxygen abundances based on the IFU (PHANGS) spectra of H II regions. The notations are the same as in Fig. A.1.

ual H II regions estimated through the S calibration, and the dark circles are the median values in bins for those data.

Appendix A.3: NGC 2835

NGC 2835 is a Sc galaxy (morphological type code T = 5.0 ± 0.4). The inclination angle of NGC 2835 is $i = 51^\circ$ (Ryder 1995), the position angle of the major axis PA = 1° (Lang et al. 2020). The optical radius is 3.30 arcmin or 198.2 arcsec (de Vaucouleurs et al. 1991). At the distance of $d = 12.22$ Mpc (Anand et al. 2021), the physical optical radius is $R_{25} = 11.74$ kpc. The stellar mass is $M_* = 1.0 \times 10^{10} M_\odot$ (Leroy et al. 2021). The mass of the central black hole in NGC 2835 is $\log M_{BH} = 6.72 \pm 0.30$ in solar mass (Davis et al. 2014). The slit spectra of H II regions in NGC 2835 were measured by Ryder (1995). Panel a of Fig. A.3 shows the oxygen abundances in those H II regions: the squares mark the $(O/H)_R$ abundances and the circles denote the $(O/H)_S$ abundances. The crosses are the median values in bins of 0.1 in fractional radius R/R_{25} . The IFU spectroscopy of NGC 2835 were carried out within the framework of the PHANGS programme and a catalog of H II regions was created (Kreckel et al. 2019). The grey circles in panel b of Fig. A.3 denote the oxygen abundances in individual H II regions estimated through the S calibration, and the dark circles are the median values in bins for those data.

Appendix A.4: NGC 2903

The nearby galaxy NGC 2903 is a Sbc spiral galaxy (morphological type code T = 4.0 ± 0.1). Its inclination angle is $i = 65^\circ$ and the position angle of the major axis PA = 204° (de Blok et al.

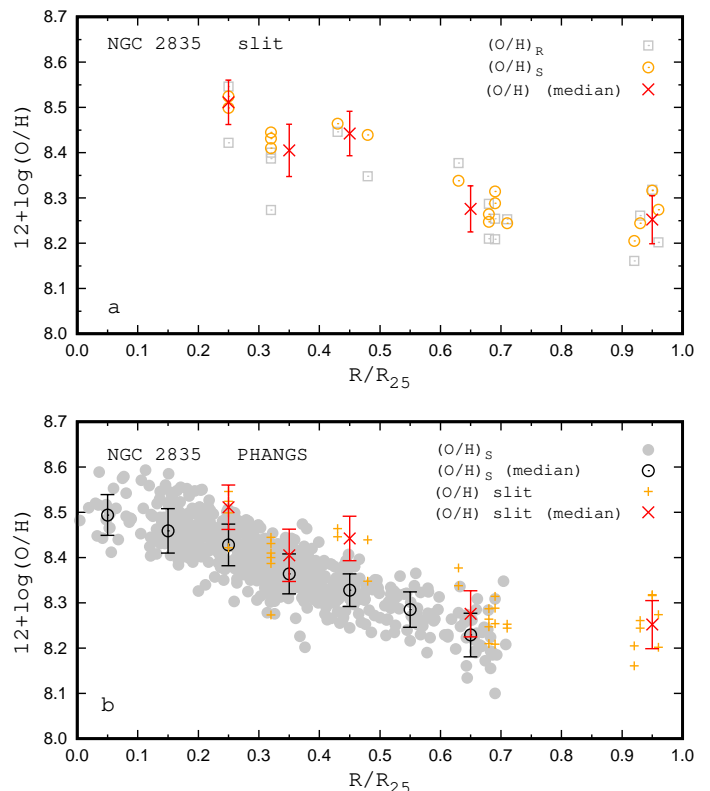


Fig. A.3. Radial oxygen abundance distribution in NGC 2835. *Panel a*: oxygen abundances based on the slit spectra of H II regions. *Panel b*: oxygen abundances based on the IFU (PHANGS) spectra of H II regions. The notations are the same as in Fig. A.1.

2008). The optical radius of NGC 2903 is $R_{25} = 5.87$ arcmin (Walter et al. 2008). The distance to NGC 2903 is $d = 8.9$ Mpc (Drozdovsky & Karachentsev 2000) that results in the physical optical radius of $R_{25} = 15.21$ kpc. The mean value of the estimations of the stellar mass of NGC 2903 (rescaled to the adopted distance) is $M_* = 3.33 \times 10^{10} M_\odot$ (Jarrett et al. 2019; Leroy et al. 2021). NGC 2903 hosts a supermassive black hole of mass $\log M_{BH} = 7.06^{+0.28}_{-7.06}$ in solar mass (van den Bosch 2016).

The slit spectra of H II regions in the disk of NGC 2903 were measured by McCall et al. (1985), van Zee et al. (1998), Bresolin et al. (2005), and Díaz et al. (2007). The squares in panel a of Fig. A.4 show the oxygen abundances estimated through the R calibration in those H II regions, and the circles denote the oxygen abundances estimated through the S calibration. The crosses are the median values in bins of 0.1 in fractional radius R/R_{25} . The IFU (fibre) spectroscopy of NGC 2903 was performed within the framework of the VENGA survey (Blanc et al. 2013; Kaplan et al. 2016). The grey points in panel b of Fig. A.4 show the IFU spectra-based $(O/H)_{S,IFU}$ abundances in the individual fibres, and the dark circles are the median values in bins for those data. Panel c of Fig. A.4 shows the same as panel b but for $(O/H)_{R,IFU}$ abundances.

Appendix A.5: NGC 4254

NGC 4254 (M 99) is a bright Sc galaxy (morphological type code T = 5.2 ± 0.7) in the Virgo Cluster. The inclination angle of NGC 4254 is $i = 34^\circ$, the position angle of the major axis PA = 68° (Lang et al. 2020). The optical radius is 2.68 arcmin (de Vaucouleurs et al. 1991). At the distance of $d = 13.1$ Mpc (Anand et al. 2021), the physical optical radius is $R_{25} = 10.23$

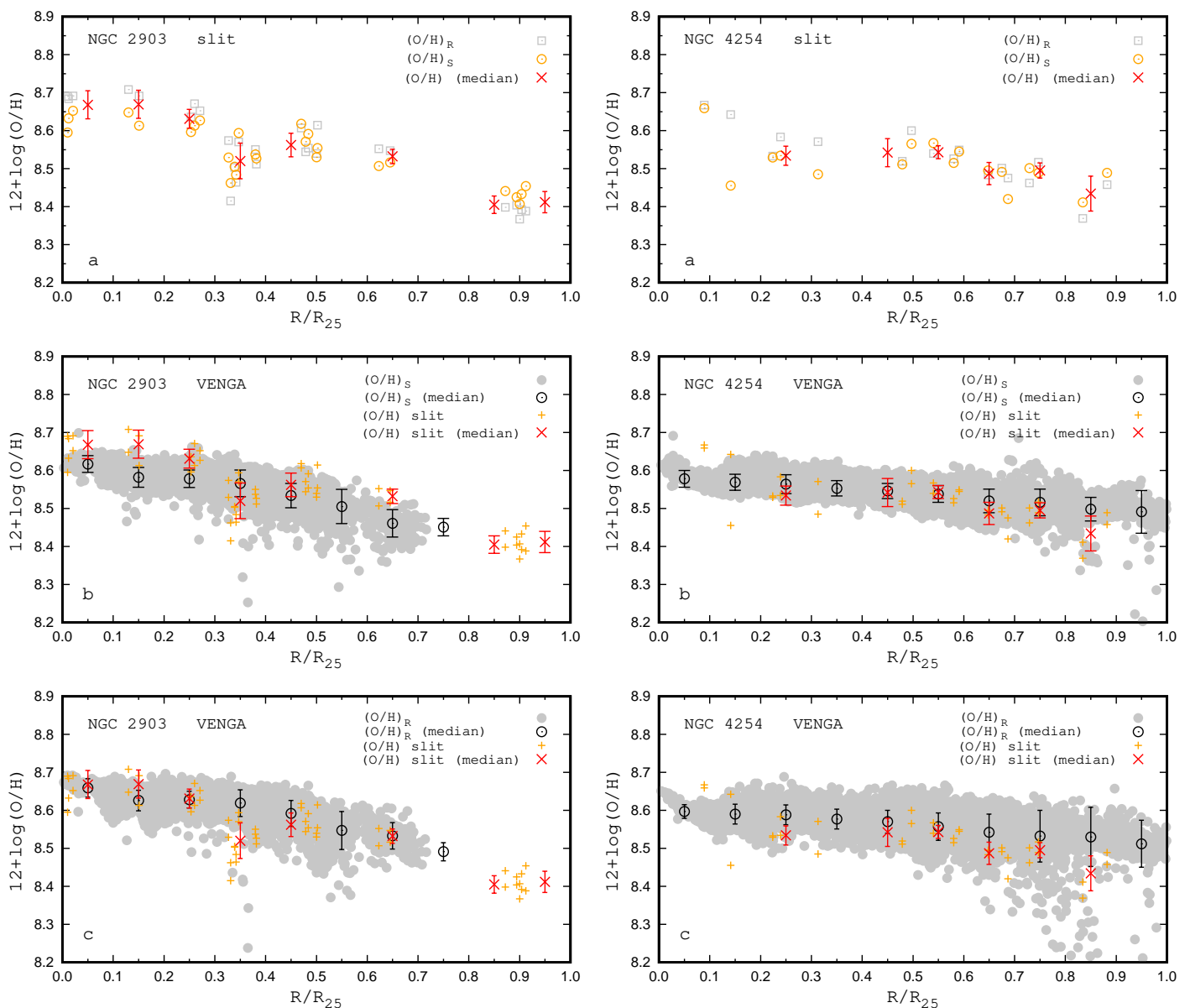


Fig. A.4. Radial oxygen abundance distribution in NGC 2903. *Panel a*: oxygen abundances based on the slit spectra of H II regions. *Panel b*: oxygen abundances estimated through the S calibration from the IFU (VENGA) spectra of fibres. *Panel c*: oxygen abundances obtained through the R calibration from the IFU (VENGA) spectra of fibres. The notations are the same as in Fig. A.1.

kpc. The stellar mass is $M_{\star} = 2.63 \times 10^{10} M_{\odot}$ (Leroy et al. 2021).

The slit spectra of H II regions in the disk of NGC 4254 were measured by McCall et al. (1985), Shields et al. (1991), and Henry et al. (1994). The squares in panel a of Fig. A.5 show the oxygen abundances estimated through the R calibration in those H II regions. The circles are the oxygen abundances estimated through the S calibration. The crosses are the median values in bins of 0.1 in fractional radius R/R_{25} . The IFU spectroscopy of NGC 4254 was carried out within the framework of the VENGA survey (Blanc et al. 2013; Kaplan et al. 2016). The grey points in panel b of Fig. A.5 show the individual fibre $(O/H)_{S,IFU}$ abundances, and the dark circles are the median values in bins for those data. Panel c of Fig. A.5 shows the same as panel b but for the $(O/H)_{R,IFU}$ abundances. The IFU spec-

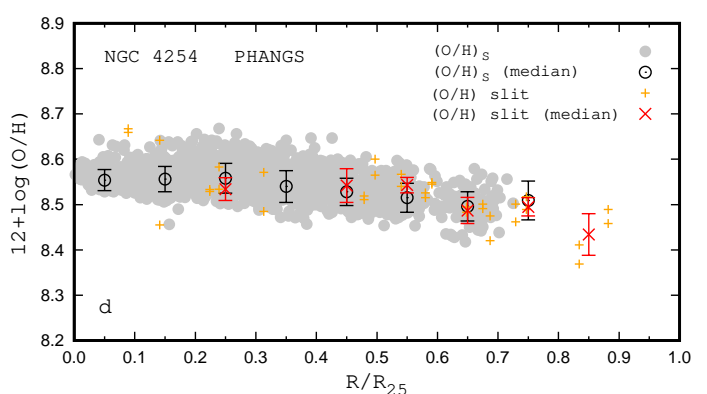


Fig. A.5. Radial oxygen abundance distribution in NGC 4254. *Panel a*: oxygen abundances based on the slit spectra of H II regions. *Panel b*: oxygen abundances estimated through the S calibration from the IFU (VENGA) spectra of fibres. *Panel c*: oxygen abundances obtained through the R calibration from the IFU (VENGA) spectra of fibres. *Panel d*: oxygen abundances estimated through the S calibration from the IFU (PHANGS) spectra of H II regions. The notations are the same as in Fig. A.1.

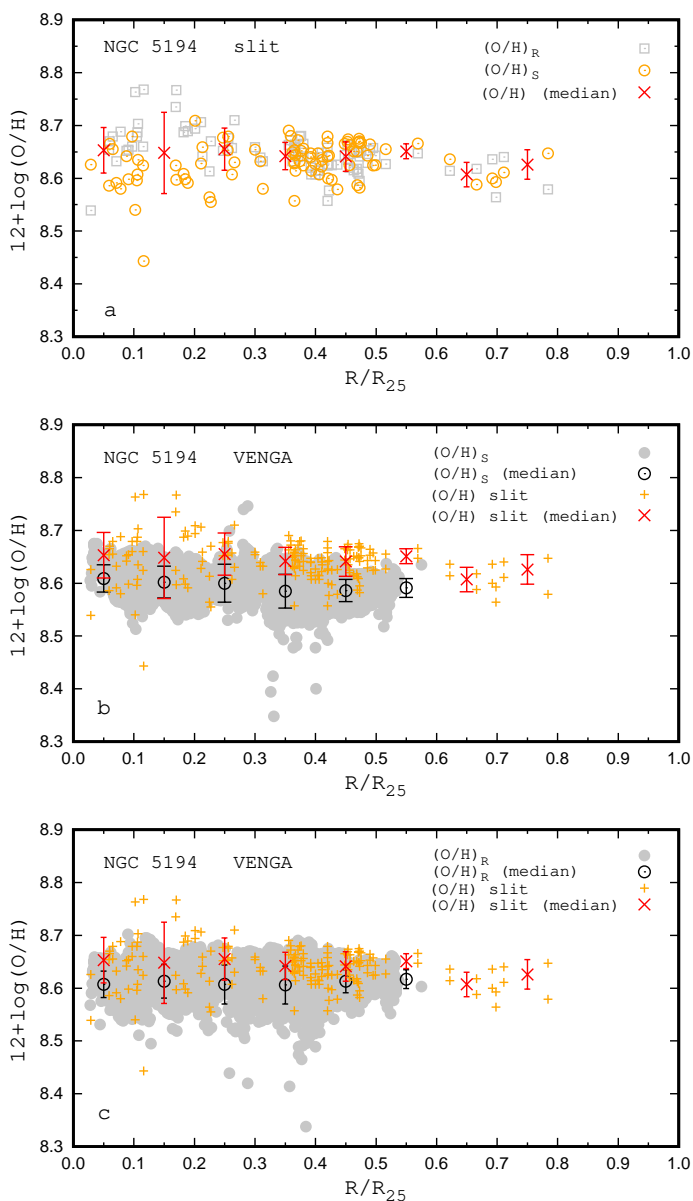


Fig. A.6. Radial oxygen abundance distribution in NGC 5194. *Panel a*: oxygen abundances based on the slit spectra of H II regions. *Panel b*: oxygen abundances estimated through the S calibration from the IFU (VENGA) spectra of fibres. *Panel c*: oxygen abundances obtained through the R calibration from the IFU (VENGA) spectra of fibres. The notations are the same as in Fig. A.1.

troscopy of NGC 4254 was also carried out within the framework of the PHANGS programme and the catalog of H II regions is constructed (Kreckel et al. 2019). The grey points in panel d of Fig. A.5 show the $(O/H)_{S,IFU}$ abundances based on the IFU spectra of H II regions, and the dark circles are the median values in bins for those data.

Appendix A.6: NGC 5194

The nearby galaxy NGC 5194 (M 51a, the Whirlpool Galaxy) is a SABB spiral galaxy (morphological type code $T = 4.0 \pm 0.3$). The bright disk of NGC 5194 ends abruptly at about 5 arcmin radius in both the optical images and the H I. The velocity structure of the gas in NGC 5194 is extremely complicated and difficult to interpret (Rots et al. 1990). There is the misalignment

of the major axes of the H I distribution and the velocity field. Therefore the geometrical parameters of NGC 5194 are rather uncertain. Tamburro et al. (2008) derive the following geometrical projection parameters of the NGC 5194 galactic disk: position angle $PA = 172^\circ$ and inclination $i = 42^\circ$. Colombo et al. (2014) undertake a detailed kinematic study of NGC 5194 and found a position angle $PA = (173 \pm 3)^\circ$, and an inclination $i = (22 \pm 5)^\circ$. The geometrical parameters of NGC 5194 obtained by Colombo et al. (2014) are used here. We adopt the optical radius of NGC 5194 to be $R_{25} = 5.61$ arcmin (de Vaucouleurs et al. 1991). It should be noted that the value of the optical radius of $R_{25} = 3.88$ arcmin is used for NGC 5194 within The H I Nearby Galaxy Survey (THINGS) (Walter et al. 2008). There are recent distance estimations for NGC 5194 through the tip of the red giant branch (TRGB) method based on the Hubble Space Telescope measurements. We adopt here the distance to NGC 5194 as $d = 8.58$ Mpc, obtained by McQuinn et al (2017). The optical radius of NGC 5194 is $R_{25} = 14.00$ kpc with adopted distance. The stellar mass rescaled to the adopted distance is $M_* = 4.54 \times 10^{10} M_\odot$ (Leroy et al. 2008; Jarrett et al. 2019).

The slit spectra of H II regions in NGC 5194 were measured in a number of works (McCall et al. 1985; Díaz et al. 1991; Bresolin et al. 1999, 2004; Garnett et al. 2004; Croxall et al. 2015). Panel a of Fig. A.6 shows the oxygen abundances estimated through the R calibration (squares) and through the S calibration (circles) in those H II regions. The crosses are the median values in bins of 0.1 in fractional radius R/R_{25} . The IFU spectroscopy of NGC 5194 was performed within the framework of the VENGA survey (Blanc et al. 2013; Kaplan et al. 2016). The grey points in panel b of Fig. A.6 show the fibre $(O/H)_S$ abundances, and the dark circles are the median values in bins.

Appendix A.7: NGC 6946

NGC 6946 is SABc galaxy (morphological type code $T = 5.9 \pm 0.3$). The inclination angle of NGC 6946 is $i = 33^\circ$, and the position angle of the major axis $PA = 243^\circ$ (de Blok et al. 2008). The optical radius is 5.74 arcmin (de Vaucouleurs et al. 1991). At the distance of $d = 7.34$ Mpc (Anand et al. 2021), the physical optical radius is $R_{25} = 12.26$ kpc. The stellar mass (mean value) is $M_* = 2.85 \times 10^{10} M_\odot$ (Jarrett et al. 2019; Leroy et al. 2019).

The slit spectra of H II regions in NGC 6946 were measured by McCall et al. (1985), Ferguson et al. (1998), and García-Benito et al. (2010). The squares in panel a of Fig. A.7 show the oxygen abundances estimated through the R calibration (squares) and through the S calibration (circles) in those H II regions. The crosses are the median values in bins of 0.1 in fractional radius R/R_{25} . The IFU spectroscopy of NGC 6946 were carried out within the framework of the Metal-THINGS programme (Lara-López et al. 2022). Only the red spectra over the wavelength range covering 4800-9300Å were obtained. The grey circles in panel b of Fig. A.7 denote the oxygen abundances in individual fibres estimated through the S calibration, and the dark circles are the median values in bins.

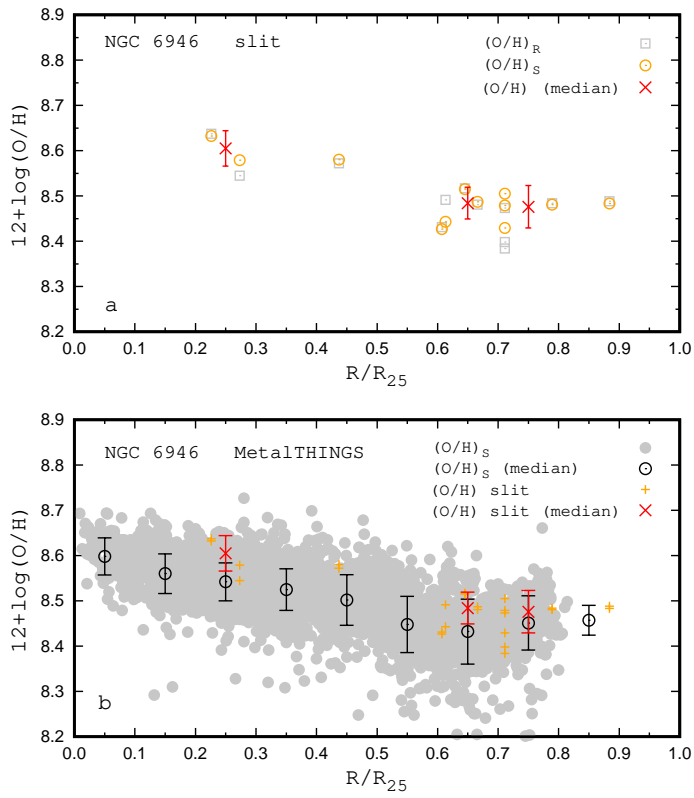


Fig. A.7. Radial oxygen abundance distribution in NGC 6946. *Panel a:* oxygen abundances based on the slit spectra of H II regions. *Panel b:* oxygen abundances estimated through the S calibration from the IFU (Metal-THINGS) spectra of fibres. The notations are the same as in Fig. A.1.